2009 Annual SCEC report

Measurements of secular and transient deformation in Southern California using InSAR data (PI: Fialko)

Publications and abstracts resulted from this project:

Wei, M., D. Sandwell and Y. Fialko, A Silent M4.8 slip event of October 3-6, 2006, on the Superstition Hills fault, Southern California, J. Geophys Res., 114, B07402, doi:10.1029/2008JB006135, 2009.

Barbot, S., Y. Fialko and D. Sandwell, Three-dimensional models of elasto-static deformation in heterogeneous media, with application to the Eastern California Shear Zone, Geophys. J. Int., 179, 500-520,doi:10.1111/j.1365-246X.2009.04194.x, 2009.

Barbot, S., Y. Fialko and Y. Bock, Postseismic deformation due to the Mw6.0 2004 Parkfield earthquake: Stress-driven creep on a fault with spatially variable rate-and-state friction parameters, J. Geophys Res., 114, B07405, doi:10.1029/2008JB005748, 2009.

Fialko, Y., Self-consistent Models of Postseismic and Interseismic Deformation due to Mature Strike-slip Faults, Eos, Trans. AGU, 90(52), Suppl., abst. T12C-01 (invited), 2009.

Summary of results:

Characterization of interseismic deformation due to the Southern San Andreas fault system using space geodetic data.

We have processed and analyzed a large set of Synthetic Aperture Radar (SAR) data from the Coachella Valley-San Bernardino-Mojave segments of the southern San Andreas Fault (SAF), as well as adjacent parts of the Eastern California Shear Zone. The analyzed data include more than 3 thousand interferograms from 4 satellite tracks spanning a time interval from 1992 until 2009. In doing so we developed new algorithms for reduction of atmospheric and other (e.g., orbital) errors in the interferometric SAR measurement. The data from different satellite tracks were combined into high-resolution mosaics of satellite line-of-sight velocity. Figure 1 illustrates results for the descending tracks 127 and 356 that span the Southern San Andreas fault system. Data shown in Figure 1 extend previously published results (*Fialko*, 2006; *Lundgren et al.*, 2009) both spatially (by including data from an overlapping track 127 to the west of the Salton Sea) and temporally (by including extra 10 years of observations between 2000 and 2009). The obtained LOS velocity field will be used (along with other available space geodetic data) to quantify "geodetic" slip rates and the effective locking depths on the Southern San Andreas and San Jacinto faults through formal inversions (including evaluation of the model uncertainties).

Development of efficient algorithms for processing of large volumes of InSAR data

Given that the main limitation to InSAR measurements of small-amplitude ground velocities associated with interseismic deformation (centimeters per year or less) is the atmospheric noise

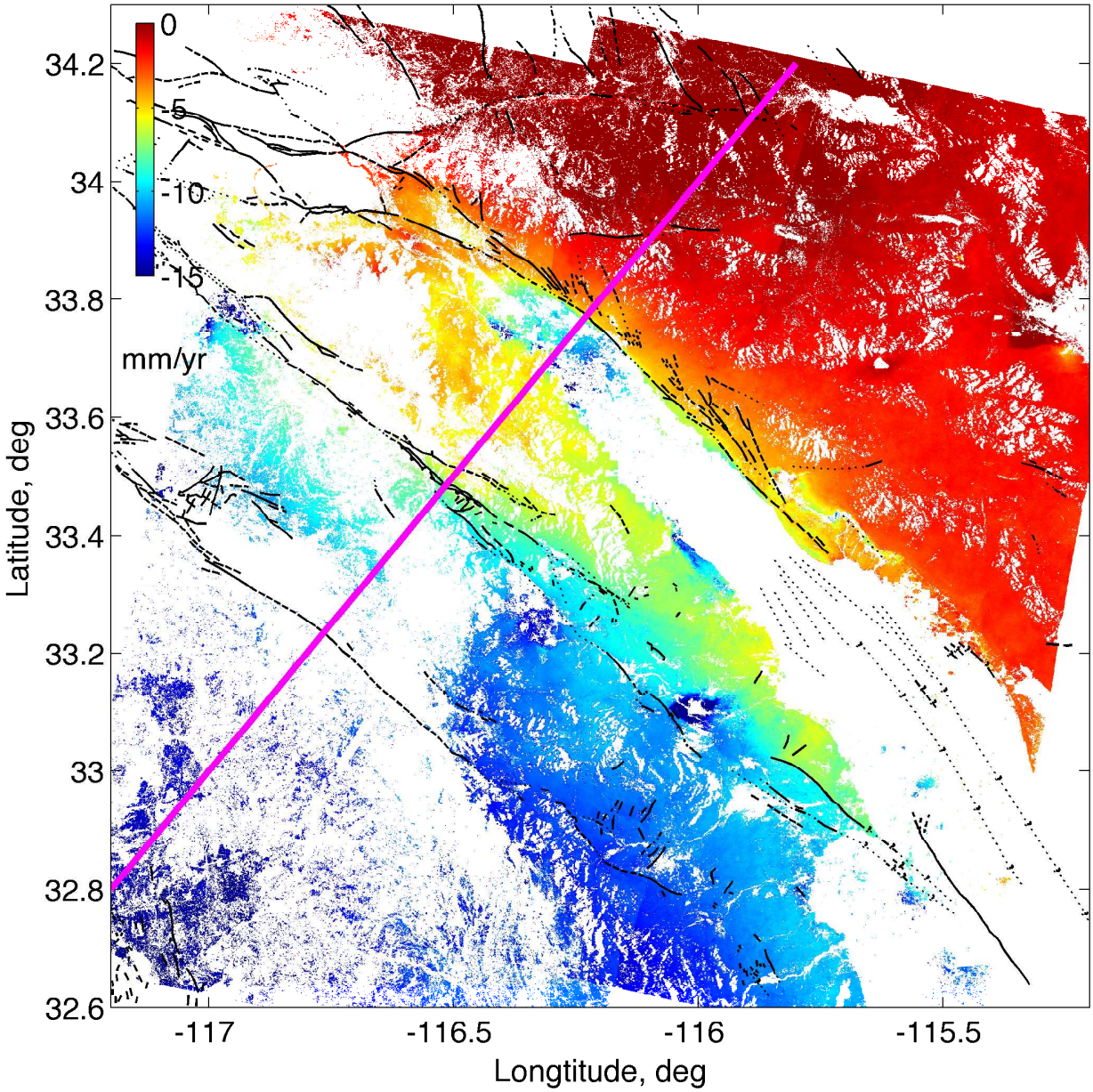

Figure 1: A mosaic of average line-of-sight (LOS) velocities derived from InSAR data from the ERS/ENVISAT tracks 127 and 356. The velocities represent deformation over a time period of 18 years between 1992 and 2009. Black wavy lines denote active faults.

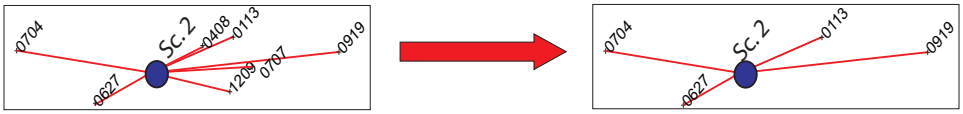

Figure 2: Partial elimination of interferograms that cancels a contribution of a "noisy" SAR scene.

(*Goldstein*, 1995; *Tarayre and Massonnet*, 1996; *Zebker et al.*, 1997), we are taking advantage of redundancy of SAR acquisitions to improve the signal-to-noise ratio. Toward this end, we have developed new algorithms for stacking of multiple interferograms and recovery of timeseries of the LOS displacements, which can effectively push InSAR technique toward the theoretical accuracy for the line of sight (LOS) velocities of order of 10^{-3} m/yr (e.g., *Berardino et al.*, 2002; *Fialko and Simons*, 2001; *Peltzer et al.*, 2001). Our method makes use of the fact that the phase contribution due to atmosphere changes sign in "consecutive" interferograms that share a common acquisition. By quantifying the magnitude of the sign-flipping phase we can identify SAR acquisitions that are highly affected by the atmospheric noise, and construct an optimal "stacking tree" that minimizes the contribution of such noisy scenes. The scheme entails the following steps:

1. Generate a set of interferograms for a prescribed range of perpendicular baselines and time spans.
2. Select a subset of interferograms with sufficient correlation and coverage.
3. Evaluate Atmospheric Noise Coefficients (ANC) for each SAR acquisition. We do so by subdividing the interferometric "connectivity tree" into triplets, and computing some norm of range changes for every interferogram, as well as for sums of sequential interferograms sharing a common scene. We identify these coefficients for all shared SAR scenes in a data set.
4. Finally, we minimize the contribution of SAR acquisitions that were deemed noisy by re-arranging the "connectivity tree" around such acquisitions so that the number of "in-coming" and "out-going" connections is the same (Figure 2). Thus the contribution of noisy scenes is canceled out: interferograms involving noisy scenes are used in the stack, but such scenes do not affect the stacked radar phase. The degree of suppression (the difference between the in-coming and out-going connections) of a particular scene may be adjusted depending on the magnitude of ANC. Note that interferometric pairs affected by significant non-steady deformation - e.g., due to an earthquake - may be used for stacking upon subtracting the coseismic signal (using either a model or shorter-term coseismic interferograms). This approach is particularly efficient in case of a temporally dense catalog with SAR acquisitions that are interferable with nearest neighbors.

We have performed a comprehensive evaluation of the described algorithm by comparing results with those obtained using other techniques, as well as independent data, such as continuous GPS.

Analysis of a silent slip event of Oct. 2006 on the Superstition Hills Fault

We discovered and documented a "slow earthquake" on the Superstition Hills fault. During October of 2006, the 20-km long Superstition Hills fault (SHF) in the Salton Trough slipped aseismically, producing a maximum offset of ∼3 centimeters. This activity was first detected by a creepmeter operated by Roger Bilham of Colorado University. We investigated this using field

surveys and ERS/ENVISAT satellite data. InSAR analysis was extended to investigate the spatial and temporal variations in slip history since 1992. During a 15-year period, quasi-steady creep was found to be punctuated by at least three events of accelerated creep. The first two events were dynamically triggered by the 1992 Landers and 1999 Hector Mine earthquakes. In contrast, there was no obvious triggering mechanism for the October 2006 event. We showed that field measurements of fault offsets after the 1999 and 2006 events are in good agreement with the InSAR data. Such an agreement indicates that creep occurred along the extremely localized (down to a millimeter scale) 20 km-long slip surface in the top 4 km of the upper crust, with maximum slip occurring at the surface. The moment released during this event is equivalent to a $M_w 4.7$ earthquake. This event produced no detectable aftershocks and was not recorded by the continuous GPS stations that were 9 km away. Modeling of the long-term creep from 1992 to 2007 creep using stacked ERS interferograms shows a maximum creep depth of 2-4 km with slip tapering with depth, in a broad agreement with slip distribution inferred for the 2006 creep event. Considering that the sediment thickness varies between 3 km and 5 km along the SHF, our results are consistent with previous studies suggesting that shallow creep is controlled by sediment depth, possibly due to induced high pore pressures in unconsolidated sediments (see *Wei et al.*, 2009, for details).

References

Berardino, P., G. Fornaro, R. Lanari, and E. Sansosti, A new algorithm for surface deformation monitoring based on small baseline differential SAR interferograms, *IEEE Trans. Geosci. Rem. Sens.*, *40*, 2375–2383, 2002.

Fialko, Y., Interseismic strain accumulation and the earthquake potential on the southern San Andreas fault system, *Nature*, *441*, 968–971, 2006.

Fialko, Y., and M. Simons, Evidence for on-going inflation of the Socorro magma body, New Mexico, from Interferometric Synthetic Aperture Radar imaging, *Geophys. Res. Lett.*, *28*, 3549–3552, 2001.

Goldstein, R. M., Atmospheric limitations to repeat-track radar interferometry, *Geophys. Res. Lett.*, *22*, 2517–2520, 1995.

Lundgren, P. E., A. Hetland, Z. Liu, and E. J. Fielding, Southern San Andreas-San Jacinto fault system slip rates estimated from earthquake cycle models constrained by GPS and interferometric synthetic aperture radar observations, *J. Geophys. Res.*, *114*, B02,403, doi:10.1029/2008JB005,996, 2009.

Peltzer, G., F. Crampe, S. Hensley, and P. Rosen, Transient strain accumulation and fault interaction in the Eastern California shear zone, *Geology*, *29*, 975–978, 2001.

Tarayre, H., and D. Massonnet, Atmospheric propagation heterogeneities revealed by ERS-1 interferometry, *Geophys. Res. Lett.*, *23*, 989–992, 1996.

Wei, M., D. Sandwell, and Y. Fialko, A silent M4.8 slip event of October 3-6, 2006, on the Superstition Hills fault, Southern California, *J. Geophys. Res.*, doi:10.1029/2008JB006135, in press, 2009.

Zebker, H. A., P. A. Rosen, and S. Hensley, Atmospheric effects in interferometric synthetic aperture radar surface deformation and topographic maps, *J. Geophys. Res.*, *102*, 7547–7563, 1997.